RESEARCH ARTICLE

HIGH-PRESSURE PHYSICS

Observation of the Wigner-Huntington transition to metallic hydrogen

Ranga P. Dias and Isaac F. Silvera*

Producing metallic hydrogen has been a great challenge in condensed matter physics. Metallic hydrogen may be a room-temperature superconductor and metastable when the pressure is released and could have an important impact on energy and rocketry. We have studied solid molecular hydrogen under pressure at low temperatures. At a pressure of 495 gigapascals, hydrogen becomes metallic, with reflectivity as high as 0.91. We fit the reflectance using a Drude free-electron model to determine the plasma frequency of 32.5 ± 2.1 electron volts at a temperature of 5.5 kelvin, with a corresponding electron carrier density of 7.7 ± 1.1 × 10^{23} particles per cubic centimeter, which is consistent with theoretical estimates of the atomic density. The properties are those of an atomic metal. We have produced the Wigner-Huntington dissociative transition to atomic metallic hydrogen in the laboratory.

Several key problems in physics involving hydrogen include production of the metallic phase, high-temperature superconductivity, and controlled nuclear fusion (*1*). The transition to solid metallic hydrogen (SMH) was envisioned by Wigner and Huntington (WH) more than 80 years ago (*2*). They predicted a first-order dissociative transition to an atomic lattice through compression of solid molecular hydrogen to a sufficiently high density. Solid atomic hydrogen would be a metal with one electron per atom with a half-filled conduction band. Although WH's density for the transition was approximately correct, their predicted pressure of 25 GPa (100 GPa = 1 megabar) was way off because they incorrectly used the zero-pressure compressibility for all pressures. Wigner and Huntington predicted a simple phase diagram. Enormous experimental and theoretical developments dramatically reshaped the phase diagram of hydrogen (Fig. 1) over the past decades. Modern quantum Monte-Carlo methods and density functional theory predict pressures of ~400 to 500 GPa for the transition (*3*–*5*), with an atomic lattice being in the $I4_1/amd$ space group (*5*, *6*). Metallic hydrogen (MH) may be a high-temperature superconductor, predicted by Ashcroft (*7*), with critical temperatures possibly higher than room temperature (*8*, *9*). Moreover, other predictions suggest SMH is metastable at room temperature when the pressure is released (*10*). The combination of these expected properties makes SMH important for solving energy problems and can potentially revolutionize rocketry as a powerful propellant (*11*).

The pathways to MH require either increasing pressure at low temperature (Fig. 1, pathway I) or increasing temperature to cross the plasma phase transition (Fig. 1, pathway II) (*12*–*17*). Pathway I transitions through a number of phases not envisioned in the simple phase diagram predicted by WH. The low-pressure properties of solid molecular hydrogen are fascinating, and many aspects—such as the importance of ortho-para concentrations, and solid-solid phase transitions characterized by orientational order—have been reviewed elsewhere (*3*, *18*). In the low-pressure, low-temperature phase I, molecules are in spherically symmetric quantum states and form a hexagonal close-packed structure. Phases II, III, and IV are phases with structural changes and orientational order of the molecules (*19*–*23*). A new phase in hydrogen observed at liquid-helium temperatures believed to precede the metallic phase was called H_2-PRE (*24*) [also named VI at higher temperatures (*25*)].

We carried out a rigorous strategy to achieve the higher pressures needed to transform hydrogen to SMH in a diamond anvil cell (DAC). Diamond failure is the principal limitation for achieving the required pressures to observe SMH. We believe that one point of failure of diamonds arises from microscopic surface defects created in the polishing process. We used type IIac conic synthetic diamonds (supplied by Almax-Easylab) with ~30-μm-diameter culet flats. We etched off ~5 μm from the diamond culets using reactive ion etching to remove surface defects (figs. S7 and S8) (*26*). We vacuum annealed the diamonds at high temperature to remove residual stresses. A second point of failure is diamond embrittlement from hydrogen diffusion. Hydrogen can disperse into the confining gasket or the diamonds (at high pressure or temperature). As an activated process, diffusion is suppressed at low temperatures. We maintained the sample at liquid-nitrogen or liquid-helium temperatures during the experimental runs. Alumina is also known to act as a diffusion barrier against hydrogen. We coated the diamonds along with the mounted rhenium (Re) gasket with a 50-nm-thick layer of amorphous alumina through the process of atomic layer deposition. We have found through our extensive experience with alumina coatings at high pressures that it does not affect or contaminate the sample, even at temperatures as high as ~2000 K (*12*). Last, focused laser beams, even at low laser power (10 mW) on samples at high pressures in DACs, can also lead to failure of the highly stressed diamonds. Laser light in the blue spectral region appears to be particularly hazardous because it potentially induces the growth of defects (*27*). Thermal shock to the stressed culet region from inadvertent laser heating is another risk. Moreover, a sufficiently intense laser beam, even at infrared (IR) wavelengths, can graphitize the surface of the diamond. Thus, we studied the sample mainly with very low-power, incoherent IR radiation from a thermal source and minimized illumination of the sample with lasers when the sample was at very high pressures.

We cryogenically loaded the sample chamber at 15 K, which included a ruby grain for pressure determination. We initially determined a pressure of ~88 GPa by means of ruby fluorescence (*26*). Determining the pressure in the megabar regime is more challenging (*26*). We measured the IR vibron absorption peaks of hydrogen at higher pressures (>135 GPa) with a Fourier transform IR spectrometer with a thermal IR source, using the known pressure dependence of the IR vibron peaks for pressure determination (*26*). We did this to a pressure of ~335 GPa, while the sample was still transparent (Fig. 2A). The shift of the laser-excited Raman active phonon of the diamond in the highly stressed culet region is currently the method used for determining pressure at extreme high pressures. For fear of diamond failure due to laser illumination and possible heating of the black sample, we only measured the Raman active phonon at the very highest pressure of the experiment (495 GPa) after the sample transformed to metallic hydrogen and reflectance measurements had been made. We equipped our DACS with strain gauges that allowed us to measure the applied load, which we found was proportional to pressure during calibration runs (*26*). We estimated pressure between 335 and 495 GPa using this calibration. We increased the load (pressure) by rotating a screw with a long stainless-steel tube attached to the DAC in the cryostat. Increasing the pressure by rotating the screw after the 335-GPa

Lyman Laboratory of Physics, Harvard University, Cambridge, MA 02138, USA.
*Corresponding author. Email: silvera@physics.harvard.edu

pressure point resulted in our sample starting to turn black (Fig. 2B) as it transitioned into the H_2-PRE phase (*24*). Earlier studies of hydrogen reported the sample as black at lower pressures (*28*), but we believe that this is a result of different pressure calibrations in this high-pressure region (*26*).

After some more screw turns (fig. S3), the sample reflectance changed from black to high reflectivity, characteristic of a metal (Fig. 2C). We then studied the wavelength dependence of the reflectance of the sample at liquid-nitrogen and liquid-helium temperatures (Fig. 3). In order to do this, the stereo microscope, used for visual observation (Fig. 2), was replaced with a high-resolution long-working-distance microscope (Wild Model 420 Macroscope) that not only allowed visual observation but also allowed an attenuated laser beam to be cofocused with the microscope image. In order to measure the reflectance, we wanted to magnify the image of the sample and project it on a camera. The Macroscope (fig. S5) (*26*) enables an external image to be formed that can be further magnified for a total calibrated magnification of ~44; this was imaged onto a color CMOS (complementary metal-oxide semiconductor) camera (DC1645C, Thorlabs). We can select the area of interest (effectively spatial filtering) and measure the reflectance from different surfaces (fig. S6). We measured the reflectance from the MH and the Re gasket. We measured at three wavelengths in the visible spectral region, using both broadband white light and three narrow band lasers that illuminated the sample (*26*), as well as one wavelength in IR. The measured reflectances are shown in Fig. 3, along with measurements of reflectance of the Re gasket and reflectance from a sheet of Re at ambient conditions that agreed well with values from the literature (*29*).

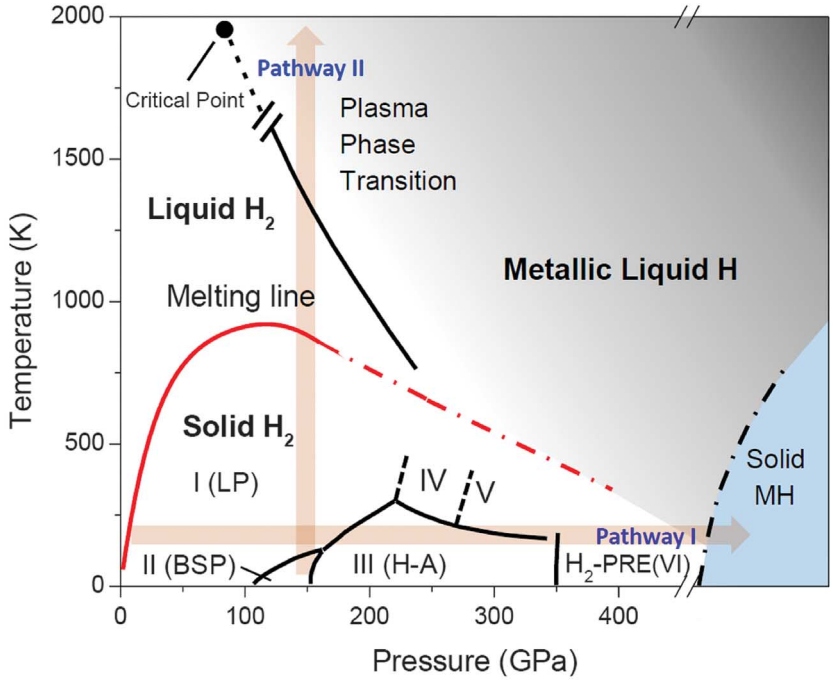

Fig. 1. Experimental/theoretical P-T phase diagram of hydrogen. Shown are two pathways to MH: I is the low-temperature pathway, and II is the high-temperature pathway. In pathway I, phases for pure para hydrogen have lettered names: LP, low pressure; BSP, broken symmetry phase; and H-A, hydrogen-A. The plasma phase transition is the transition to liquid metallic atomic hydrogen.

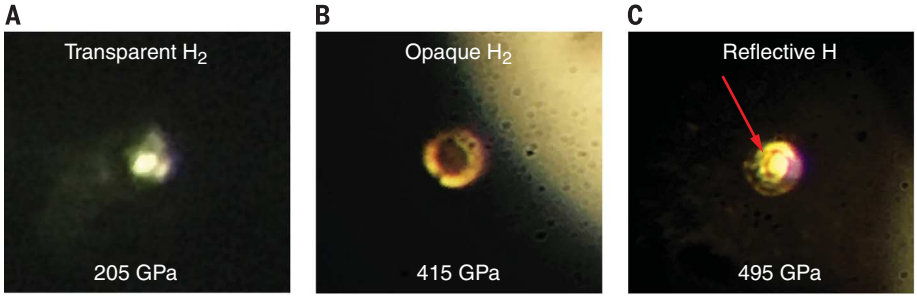

Fig. 2. Photographs of hydrogen at different stages of compression. Photos were taken with an iPhone camera (Apple, Cupertino, CA) at the ocular of a modified stereo microscope, using light-emitting diode (LED) illumination in the other optical path of the microscope. (**A**) At pressures up to 335 GPa, hydrogen was transparent. The sample was both front and back illuminated in this and in (B); the less bright area around the sample is light reflected off of the Re gasket. (**B**) At this stage of compression, the sample was black and nontransmitting. The brighter area to the top right corner is due to the LED illumination, which was not focused on the sample for improved contrast. (**C**) Photo of metallic hydrogen at a pressure of 495 GPa. The sample is nontransmitting and observed in reflected light. The central region is clearly more reflective than the surrounding metallic Re gasket. The sample dimensions are ~8 to 10 μm, with thickness of ~1.2 μm (*26*).

At high pressure, the stressed culet of the diamond becomes absorptive, owing to closing down of the diamond band gap (5.5 eV at ambient) (*30*). This attenuated both the incident and reflected light and is strongest in the blue. Fortunately, this has been studied in detail by Vohra (*31*), who provided the optical density for both type I and II diamonds to very high pressures. We used this study (fig. S4) and determined the corrected reflectance (Fig. 3A). Last, after we measured the reflectance, we used very low laser power (642.6 nm laser wavelength) and measured the Raman shift of the diamond phonon to be 2034 cm^{-1}. This value fixes the end point of our rotation or load scale because the shift of the diamond phonon line has been calibrated. The linear 2006 scale of Akahama and Kawamura (*32*) gives a pressure of 495 ± 13 GPa when the sample was metallic. We do not include the potentially large systematic uncertainty in the pressure (*26*). This is the highest pressure point on our pressure versus load or rotation scale (fig. S3). Such curves eventually saturate; the pressure does not increase as the load is increased.

An analysis of the reflectance can yield important information concerning the fundamental properties of a metal. A very successful and easy-to-implement model is the Drude free-electron model of a metal (*33*). This model of a metal is likely a good approximation to relate reflectance to fundamental properties of a metal. A recent band structure analysis of the $I4_1/amd$ space group by Borinaga *et al.* (*9*) shows that for this structure, electrons in SMH are close to the free-electron limit, which supports the application of a Drude model. The Drude model has two parameters, the plasma frequency ω_p and the relaxation time τ. The plasma frequency is given by $\omega_p^2 = 4\pi n_e e^2/m_e$, where m_e and e are the electron mass and charge and n_e is the electron density. The complex index of refraction of MH is given by $N_H^2 = 1 - \omega_p^2/(\omega^2 + j\omega/\tau)$, where ω is the angular frequency of the light. The MH is in contact with the stressed diamond that has an index of refraction N_D; this has a value of ~2.41 in the red region of the spectrum at ambient

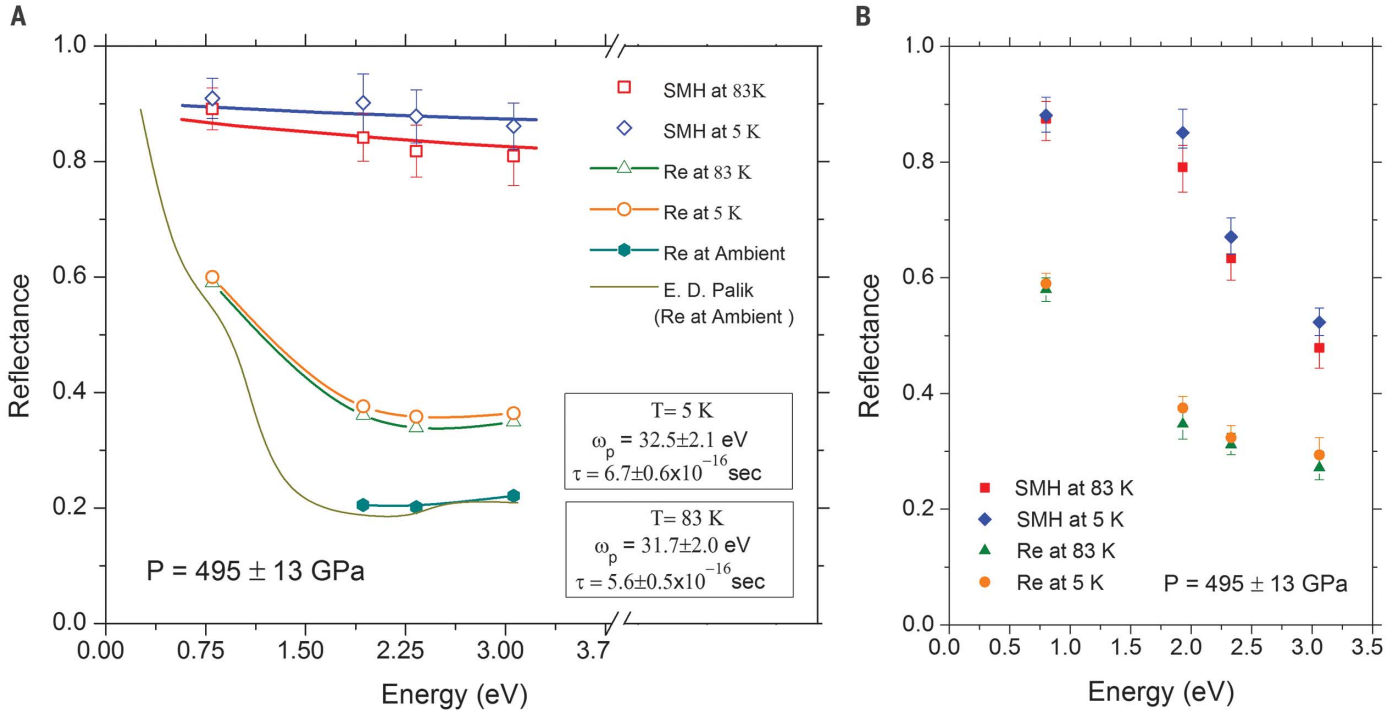

Fig. 3. Reflectance as a function of photon energy. (**A**) The energy dependence of the normal incidence reflectance off MH and the Re gasket, *P* = 495 GPa, at liquid-nitrogen and liquid-helium temperatures. We also show our measured reflectance from a surface of Re at a pressure of 1 bar at room temperature; this is in good agreement with literature values, verifying our measurement procedure. The reflectances have been corrected for absorption in the diamond. The lines through MH data are fits with a Drude free-electron model; the lines through the Re data points are guides to the eye. (**B**) Raw reflectance data without the diamond absorption correction. The uncertainties in the data points are from measurement of the reflectance and the correction procedure and represent random errors.

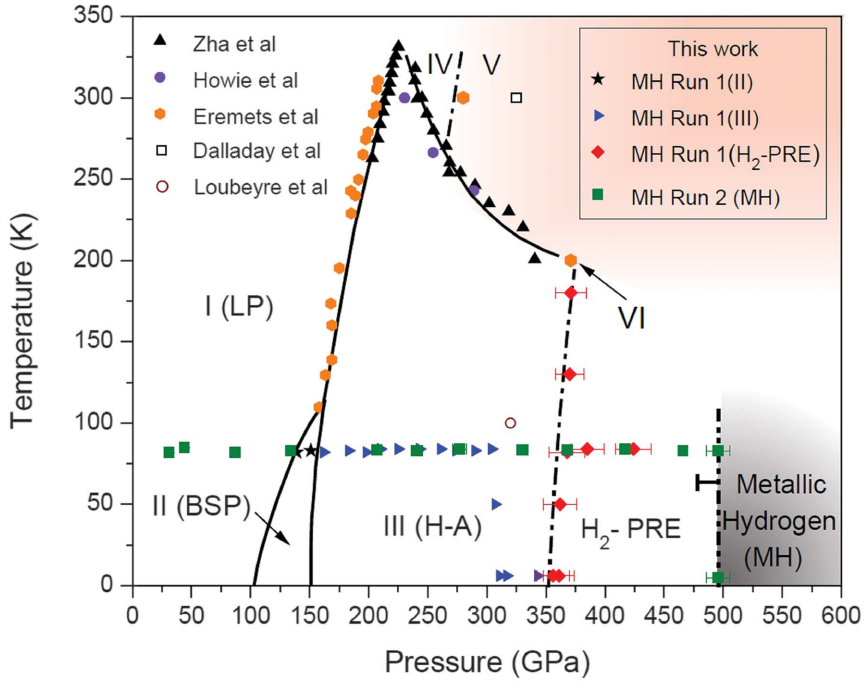

Fig. 4. The T-P phase diagram of hydrogen along pathway I of Fig. 1. The data show the thermodynamic pathway followed for our measurements. We also show other recent data for the phases at lower pressures from Zha *et al*. (*41*), Howie *et al*. (*23*), Eremets *et al*. (*25*), and Dias *et al*. (*24*). A transition claimed by Dalladay-Simpson *et al*. (*42*) at 325 GPa is plotted as a point, as is the earlier observation of black hydrogen by Loubeyre *et al*. (*28*).

conditions. We measured reflectance $R(\omega) = |(N_D - N_H)/(N_D + N_H)|^2$ as a function of energy or (angular) frequency ω. We used a least-squares fit to the corrected reflectance data to determine the Drude parameters at 5 K, 32.5 ± 2.1 eV, and 6.7 ± 0.6 × 10^{16} s. These values differ appreciably from a fit to the uncorrected data.

Because the diamond culet is stressed, we expect the index of refraction in the region of contact with the MH to change from the value at ambient pressure, and this might lead to an important uncertainty in the fitting parameters. The index of the diamond under pressure and uniaxial stress has been studied by Surh *et al*. (*34*). For hydrostatic pressures up to 450 GPa, the pressure dependence is rather weak; however, for uniaxial stressed diamond the change of index can be substantial. We fitted data for values of 2.12 for extreme uniaxial stress along the [001] crystal direction and 2.45 along the [100] and [010] directions, corresponding to a sample pressure of 250 GPa (*34*). This resulted in an uncertainty in the Drude parameters that was much smaller than that because of the uncertainty in the measured reflectance (Fig. 3). We fit the reflectance using a value N_D = 2.41, yielding the values for the Drude parameters shown in Fig. 3 and Table 1.

The pressure-temperature phase diagram of hydrogen along pathway I is shown in Fig. 4, focusing on the lower-temperature region. With

Table 1. Elements of the first column of the periodic table. We compare the electron density (calculated from the plasma frequency) in the second column with the atom density in the third column and see that there is about 1 electron per atom. The plasma frequencies are from (*43*). The data are for hydrogen at 5.5 K; all other elements are at 77 K. A definition of r_s/a_0 is provided in (*26*).

Element	$n_e = \frac{m_e\omega_p^2}{4\pi e^2}$ (10^{22}/cm^3)	n_a (10^{22}/cm^3)	r_s/a_o	Plasma frequency (eV)
Hydrogen	77 ± 11	66.5 to 86.0	1.255 to 1.34	32.5 ± 2.1
Lithium	3.68	4.63	3.25	7.12
Sodium	2.36	2.54	3.93	5.71
Potassium	1.00	1.33	4.86	3.72

increasing pressure, hydrogen enters the phase H_2-PRE at 355 GPa, and this is followed by the phase line based on the two points at temperature (T) = 83 and 5.5 K for the transition to MH. (*24*). Because we changed the pressure in larger increments by rotating a screw, there could be a systematic uncertainty of ~25 GPa on the low-pressure side of the phase line. The transition to MH may have taken place while increasing the pressure from ~465 to 495 GPa (*26*). We believe that the metallic phase is most likely solid, based on recent theory (*35*), but we do not have experimental evidence to discriminate between the solid and liquid states. We detected no visual change in the sample when the temperature was varied between 83 and 5.5 K. A theoretical analysis predicted a maximum in the pressure-temperature melting line of hydrogen (*36*). The maximum was first experimentally observed by Deemyad and Silvera (*37*). One speculation has the melting line (Fig. 1) extrapolating to the T = 0 K limit at high pressure, resulting in liquid MH in this limit (*10*, *36*). An extrapolation of the negative P,T slope was supported by a calculation (*38*) showing that the liquid atomic phase might be the ground state in the low-temperature limit. On the other hand, Zha (*39*) has extended the melting line to 300 GPa and finds a slope that is shallower than the extrapolation shown in Fig. 1. The vibron spectra at low temperature in phase H_2-PRE correspond to spectra from a solid. Although H_2-PRE is solid, the possibility remains that an increase in translational zero-point energy occurs when molecular hydrogen dissociates, resulting in a liquid ground state.

The plasma frequency ω_p = 32.5 ± 2.1 eV is related to the electron density and yields a value of $n_e = 7.7 \pm 1.1 \times 10^{23}$ particles/cm^3. No experimental measurements exist for the atom density at 500 GPa. Theoretical estimates range from ~6.6 to 8.8 × 10^{23} particles/cm^3 (*26*). This is consistent with one electron per atom, so molecular hydrogen is dissociated, and the sample is atomic MH, or the WH phase. Whereas some predictions suggest metallization of molecular hydrogen at high pressure (*3*), this requires one electron for every two atoms instead. MH at 495 GPa is about 15-fold denser than zero-pressure molecular hydrogen. We compared MH with other elements in the first column of the periodic table (Table 1), which has a remarkable contrast in properties.

We have produced atomic MH in the laboratory at high pressure and low temperature. MH may have an important impact on physics and perhaps will ultimately find wide technological application. Theoretical work suggests a wide array of interesting properties for MH, including high-temperature superconductivity and superfluidity (if a liquid) (*40*). A looming challenge is to quench MH and if so, study its temperature stability to see whether there is a pathway for production in large quantities.

REFERENCES AND NOTES

1. V. L. Ginzburg, *Rev. Mod. Phys.* **76**, 981–998 (2004).
2. E. Wigner, H. B. Huntington, *J. Chem. Phys.* **3**, 764–770 (1935).
3. J. M. McMahon, M. A. Morales, C. Pierleoni, D. M. Ceperley, *Rev. Mod. Phys.* **84**, 1607–1653 (2012).
4. J. McMinis, R. C. Clay, D. Lee, M. A. Morales, *Phys. Rev. Lett.* **114**, 105305 (2015).
5. S. Azadi, B. Monserrat, W. M. C. Foulkes, R. J. Needs, *Phys. Rev. Lett.* **112**, 165501 (2014).
6. J. M. McMahon, D. M. Ceperley, *Phys. Rev. Lett.* **106**, 165302–165304 (2011).
7. N. W. Ashcroft, *Phys. Rev. Lett.* **21**, 1748–1749 (1968).
8. J. M. McMahon, D. M. Ceperley, *Phys. Rev. B* **84**, 144515 (2011).
9. M. Borinaga, I. Errea, M. Calandra, F. Mauri, A. Bergara, *Phys. Rev. B* **93**, 174308 (2016).
10. E. G. Brovman, Y. Kagan, A. Kholas, *Sov. Phys. JETP* **34**, 1300–1315 (1972).
11. J. Cole, I. F. Silvera, J. P. Foote, Conceptual launch vehicles using metallic hydrogen propellant. *AIP Conf. Proc. 978*, M. S. El-Genk, Ed. (STAIF-2008, 2008), pp. 977–984.
12. M. Zaghoo, A. Salamat, I. F. Silvera, *Phys. Rev. B* **93**, 155128 (2016).
13. S. T. Weir, A. C. Mitchell, W. J. Nellis, *Phys. Rev. Lett.* **76**, 1860–1863 (1996).
14. V. E. Fortov *et al.*, *Phys. Rev. Lett.* **99**, 185001–185004 (2007).
15. M. D. Knudson *et al.*, *Science* **348**, 1455–1460 (2015).
16. C. Pierleoni, M. A. Morales, G. Rillo, M. Holzmann, D. M. Ceperley, *Proc. Natl. Acad. Sci. U.S.A.* **113**, 4953–4957 (2016).
17. G. E. Norman, I. M. Saitov, V. V. Stegailov, *Plasma Phys.* **55**, 215–221 (2015).
18. I. F. Silvera, *Rev. Mod. Phys.* **52**, 393–452 (1980).
19. I. F. Silvera, R. J. Wijngaarden, *Phys. Rev. Lett.* **47**, 39–42 (1981).
20. R. J. Hemley, H. K. Mao, *Phys. Rev. Lett.* **61**, 857–860 (1988).
21. H. E. Lorenzana, I. F. Silvera, K. A. Goettel, *Phys. Rev. Lett.* **63**, 2080–2083 (1989).
22. M. I. Eremets, I. A. Troyan, *Nat. Mater.* **10**, 927–931 (2011).
23. R. T. Howie, C. L. Guillaume, T. Scheler, A. F. Goncharov, E. Gregoryanz, *Phys. Rev. Lett.* **108**, 125501 (2012).
24. R. Dias, O. Noked, I. F. Silvera, New low temperature phase transition in dense hydrogen: The phase diagram to 421 GPa; arXiv:1603.02162v1 (2016).
25. M. I. Eremets, I. A. Troyan, A. P. Drozdov, Low temperature phase diagram of hydrogen at pressures up to 380 GPa. A possible metallic phase at 360 GPa and 200 K; https://arxiv.org/abs/1601.04479 (2016).
26. Materials and methods are available as supplementary materials.
27. M. I. Eremets, *J. Raman Spectrosc.* **34**, 515–518 (2003).
28. P. Loubeyre, F. Occelli, R. LeToullec, *Nature* **416**, 613–617 (2002).
29. E. D. Palik, Ed., *Handbook of Optical Constants of Solids* (Elsevier, 1997), vol. III.
30. A. L. Ruoff, H. Luo, Y. K. Vohra, *J. Appl. Phys.* **69**, 6413–6416 (1991).
31. Y. K. Vohra, in *Proceedings of the XIII AIRAPT International Conference on High Pressure Science and Technology* (World Scientific, 1991).
32. Y. Akahama, H. Kawamura, *J. Appl. Phys.* **100**, 043516 (2006).
33. F. Wooten, *Optical Properties of Solids* (Academic Press, 1972).
34. M. P. Surh, S. G. Louie, M. L. Cohen, *Phys. Rev. B Condens. Matter* **45**, 8239–8247 (1992).
35. J. Chen *et al.*, *Nat. Commun.* **4**, 2064 (2013).
36. S. A. Bonev, E. Schwegler, T. Ogitsu, G. Galli, *Nature* **431**, 669–672 (2004).
37. S. Deemyad, I. F. Silvera, *Phys. Rev. Lett.* **100**, 155701 (2008).
38. C. Attaccalite, S. Sorella, *Phys. Rev. Lett.* **100**, 114501 (2008).
39. C. S. Zha, "Hot-dense hydrogen study up to 300 GPa," presented at APS March Meeting 2016, Baltimore, MD, 17 March 2016; http://meetings.aps.org/link/BAPS.2016.MAR.V21.3.
40. E. Babaev, A. Sudbø, N. W. Ashcroft, *Nature* **431**, 666–668 (2004).
41. C.-S. Zha, Z. Liu, R. J. Hemley, *Phys. Rev. Lett.* **108**, 146402–146407 (2012).
42. P. Dalladay-Simpson, R. T. Howie, E. Gregoryanz, *Nature* **529**, 63–67 (2016).
43. C. Kittel, *Introduction to Solid State Physics* (John Wiley & Sons, ed. 7, 1996).

ACKNOWLEDGMENTS

We thank O. Noked, M. Zaghoo, R. Husband, and C. Meyers for assistance and discussions. O. Noked provided valuable assistance developing our general optical setup; R. Husband did the reactive ion etching, as well as the alumina coating of the diamonds; and M. Turner of the Walsworth group provided help for annealing our diamonds. The NSF, grant DMR-1308641, and the U.S. Department of Energy Stockpile Stewardship Academic Alliance Program, grant DE-NA0003346, supported this research. Partial support was provided by a grant from A. Silvera and K. Silvera. Preparation of diamond surfaces was performed in part at the Center for Nanoscale Systems (CNS), a member of the National Nanotechnology Infrastructure Network (NNIN), which is supported by NSF under NSF award ECS-0335765. CNS is part of Harvard University. The data reported in this paper are tabulated and available from the authors. Both authors contributed equally to all aspects of this research.

SUPPLEMENTARY MATERIALS

www.sciencemag.org/content/355/6326/715/suppl/DC1
Materials and Methods
Figs. S1 to S8
Databases S1 to S14
References (*44*–*60*)

5 October 2016; accepted 13 January 2017
Published online 26 January 2017
10.1126/science.aal1579

Editor's Summary

Stamping hydrogen into metal

In 1935, Wigner and Huntington predicted that molecular hydrogen would become an atomic metal at a pressure of 25 GPa. Eighty years and more than 400 GPa later, Dias and Silvera have finally produced metallic hydrogen at low temperature. The metallization occurred between 465 and nearly 500 GPa at 5.5 K. Spectroscopic measurements verified that hydrogen was in the atomic state. The observation completes an unexpectedly long quest to find the metallic hydrogen that Wigner and Huntington predicted so long ago.

Science, this issue p. 715

Corrected: 10 February 2017

www.sciencemag.org/cgi/content/full/science.aal1579/DC1

Supplementary Material for

Observation of the Wigner-Huntington transition to metallic hydrogen

Ranga P. Dias and Isaac F. Silvera*

*Corresponding author. Email: silvera@physics.harvard.edu

Published 26 January 2017 as *Science* First Release
DOI: 10.1126/science.aal1579

This PDF file includes:

Other Supplementary Material for this manuscript includes the following:
(available at www.sciencemag.org/content/science.aal1579/DC1)

Databases S1 to S14 as a separate .zip file

Correction: The Optical Density.csv file in the Database .zip was corrected and the Figure S4 plot was updated.

Science
AAAS

Supplementary Materials for

Observation of the Wigner-Huntington Transition to Metallic Hydrogen

Ranga P. Dias and Isaac F. Silvera

correspondence to: silvera@physics.harvard.edu

Materials and Methods

The Diamond Anvil Cell and Measurement Apparatus

High purity hydrogen gas (four 9s) was cryogenically loaded into a diamond anvil cell in a cryostat mounted on an optical table, similar to one described in Ref. (*41*), but with CaF_2 IR transmitting windows. An IR light beam from a Nicolet Fourier Transform infrared interferometer was focused onto the sample and then imaged onto an indium gallium arsenide detector used for transmission studies in the near IR. Spectra (shown ahead) confirmed that the sample was hydrogen and were used for pressure determination at intermediate pressures up to 335 GPa. The optical table also incorporated standard instrumentation to measure Raman scattering and fluorescence, including an edge filter to remove background contributions from the laser line. Synthetic conic type IIac diamonds were used. These were mounted in tungsten carbide seats with a matching conic surface. The diamonds were epoxied in place with an epoxy/nano-alumina paste to correct for any difference in the conic angles of the diamond and the seat. Culet diameters were ~30 microns with 8 degree bevels out to a diameter of 300 microns; the diamonds had a 2.5 mm girdle. The rhenium gasket was about 8 microns thick before pressurization and the hole diameter was about 24 microns. We have several DACs of similar design; the DAC was made of Vascomax and has the identity VMA. A large effort was made to insure that the diamond culets remained opposed and parallel to each other to the highest loads that were applied.

Pressure Determination

There is no standard for the determination of the pressures produced in DACs, but there are a number of methods and calibrations that are used. The high-pressure community has adopted the ruby scale in which the frequency of the peak of the ruby R1 fluorescence line is calibrated against pressure. Ruby is very useful for pressures up to 150-200 GPa, but is difficult to excite for higher pressures, although techniques exist (*42*). We have used ruby fluorescence to measure pressures up to about 88 GPa, using the scale of Chijioke et al (*43*). When improved calibrations are produced, older results can be recalibrated or scaled if the frequencies or the calibration are given for a current measurement. Thus, pressures based on the current calibrations are used to characterize new phenomena and the scale that is utilized

is given.

An example of challenges in pressure calibration is the pressure where black hydrogen is observed; in our case the sample starts darkening in the H_2-PRE phase, definitely becoming black around 400 GPa (*24*). Earlier Loubeyre et al reported black hydrogen at a pressure of ~320 GPa (*28*) using calibrations based on an extrapolation of the ruby pressure scale (*44*) that had been calibrated to 80 GPa in a non-hydrostatic medium. They evidently extrapolated from ~80 GPa to 320 GPa. By contrast Narayana et al (*45*) had observed hydrogen to be transparent to 342 GPa, based on the more accurate x-ray diffraction of their gasket; this created an important contradiction in observations. With an improved ruby pressure scale calibrated to 150 GPa (*43*), Silvera suggested (*46*) that the pressure of black hydrogen reported by Loubeyre et al might be ~60 GPa higher, resolving the contradiction.

In the past several years researchers studying hydrogen and its isotopes at extreme pressures have often used the Raman or IR peaks whose frequencies have been calibrated against pressure determined by x-ray markers. This procedure was done in this study for pressures in the range 88 to 335 GPa. In Fig. S1 we show some of the IR vibron spectra; we used the pressure dependence of the H_2 IR-vibron measured by Zha et al (*47*) to determine the pressure of our sample, and to be consistent with other measurements on hydrogen and its isotopes. More detail on this procedure can be found elsewhere (*24*).

For the highest pressures, researchers have started using the Raman scattering phonon spectra arising from the stressed region of the culet, first proposed many years ago (*48, 49*); several calibrations exist. The highest pressure calibrations have been provided by Akahama and Kawamura (*32, 50, 51*). They give an uncertainty in pressure of about 2% in their measurements (*51*) and fit their data to both linear and a quadratic curves. Baer et al (*52*) pointed out that the calibration depends on the diamond geometry and gasket, by using the vibron frequency of hydrogen or deuterium as a reference and finding a variance in the diamond Raman frequency. Howie et al (*53*) used this method to compare diamond Raman data from various groups and state a pressure scatter of about 25 GPa. Thus, we use an uncertainty of ±13 GPa. Due to these large uncertainties at higher pressures we round our pressure values to the nearest 0 or 5 GPa.

We have used the pressure scale of Akahama and Kawamura for the diamond phonon. Their latest calibrations are from the years 2006, 2007 and 2010, with highest measured pressures of 310, 370, and 410 GPa, respectively. The 2006 scale fits the pressure to a linear function of the frequency of the Raman feature, while the 2007 and 2010 fit to a quadratic equation, the same in both papers. We used the linear Raman scale to measure the pressure of metallic hydrogen. The appropriate Raman feature (minimum of the derivative of the spectrum at the high frequency edge) was 2034 cm^{-1}, shown in Fig. S2. This yields P=495 GPa for the linear fit and 590 GPa for the quadratic fit. We decided to use the linear scale for reasons discussed ahead.

The extrapolation of the diamond phonon to ~500-600 GPa is large. We decided to use an internal scale that we use in our group to help decide on whether to use the linear or quadratic scale. Our DACs enable us to measure the load (with strain gauges) vs. pressure. In general the load is proportional to the rotation of a screw that increases the load. As explained in the caption of Fig. S3, we used a pressure vs. load (or rotation) scale.

Reflectance Corrections

The unstressed diamond has a band gap of 5.5 eV. As pressure is increased the band gap narrows and at very high pressures diamond becomes absorbing in the blue region, so the diamond window begins to close down (*30*). The behavior has been studied in detail in type I and II diamonds to pressures as high as 421 GPa by Vohra (*54*). His article provides the optical density (OD) of the diamond by measuring reflectance of metals in a DAC. We measure exactly the same property, the reflectance of metallic hydrogen. Thus, we can use the values of the two-pass OD (light in and out undergoes two attenuations) to correct our measured values of the reflectance. We measure reflectance at higher pressures than the OD scale of Vohra. Using his OD curves, we linearly extrapolate to our pressure for the frequencies used in the reflectance measurements. The extrapolation is shown in Fig. S4.

Particle Density Estimates of Metallic Hydrogen

There are many estimates of the density of solid metallic hydrogen at the transition. We have used several of these, experimental and theoretical, to estimate the particle density at the pressure of the transition, which we take as 495 GPa. We give this as particle density and r_s, scaled to the Bohr radius a_0 ($1/n = (4\pi/3)(r_s a_o)^3$). Loubeyre et al measured the EOS to 109 GPa (*55*); extrapolating their fitting formula gives 8.1×10^{23} atoms/cm^3 (r_s=1.25); extrapolation of the gap to zero in Ref. (*28*) gives 8.65×10^{23} atoms/cm^3 (r_s=1.255); Ashcroft (*56*) calculated 6.65×10^{23} atoms/cm^3 (r_s=1.34); McMahon and Ceperley (*6*) calculated 8.6×10^{23} atoms/cm^3 (r_s=1.23). We summarize stating that the particle density at 495 GPa is in the range 6.65-8.6 $\times 10^{23}$ atoms/cm^3 (r_s=1.255-1.34).

Optical Setup

The optical setup used to measure the reflectance and Raman spectra of the diamond is shown in Fig. S5. A collimated beam emerging from the microscope (Wild Model 420 Macroscope) is focused by a lens; the image formed at the focus is magnified ten-fold by a second lens and imaged onto a CMOS camera. Either the CMOS camera was used for reflectance measurements or a fiber optic coupled to the spectrometer was placed at the focus of the Macroscope for Raman scattering measurements, along with an edge filter in the collimated beam emerging from the port of the Macroscope. For the reflectance measurements in the visible two other lasers could be coupled in on the same beam path as the one shown, using flip-mirrors (not shown). The beam path was determined for all lasers using separated pinholes (not shown) that the laser beams were required to pass through. For reflectance measurements in the IR the CMOS camera was replaced with an InGaAs IR detector. The IR beam was aligned through the pinholes and chopped with a mechanical chopper at the focus of the beam coming out of the Macroscope. This was tenfold magnified onto the IR detector. In front of this detector was an adjustable spatial filter aperture that sampled an area corresponding to a diameter of ~5 microns of the sample region. The Macroscope also has a white light source that illuminates the sample at the focus for viewing (Fig S6) To assure that alignment the IR measurements was proper, the reflectance of the red laser was measured without visual observation of focusing on the sample. A lock-in amplifier, synchronized to the chopper, was used for these measurements. Not shown is the stereo microscope that could replace the Macroscope, initially used for visually monitoring the sample and photographing it.

Sample Dimensions

We estimate the thickness of metallic hydrogen as follows. The starting dimensions of the gasket hole were diam=24 μ and thickness=8 μ. At the highest pressure the metallic hydrogen sample was oval shaped with the length of the major axis being ~10 microns, measured with the Macroscope. The final density was ~15 times greater than the zero pressure density. This yields a final thickness of ~1.2 microns, assuming no loss of sample.

Pathway II. Liquid Metallic Hydrogen.

Recently liquid metallic hydrogen (LMH) has been produced at static pressures in a DAC, with a determination of the T-P phase line shown in Fig. 1 (*12*). Earlier, Weir et al (*13*) observed LMH in a shock experiment, however they saw a continuous change from insulating to metallic conductivity. Subsequently a number of shock experiments have been carried out, mainly on deuterium, observing metallic reflectance (*14, 15, 21, 57-60*). Other research (62) disputes the findings of metallic behavior, but reanalysis of their measurements can resolve the conflicting observations (63).

Reactive Ion Etching

The mechanically polished surfaces of the culets of diamonds were examined with atomic force microscopy (AFM). This revealed the presence of polishing defects shown in Fig. S7. A Plasma-Therm Versaline RIE system http://www.plasma-therm.com/versaline-rie.html housed in the clean room of the Harvard Center for Nanoscale Sciences (CNS) was used to etch about 5 microns from the diamond to remove surface and subsurface defects created by polishing (Fig. S8). Proper etching of diamonds has challenges as the etching rate is anisotropic. An etching program can remove defects or create pits where defects existed.

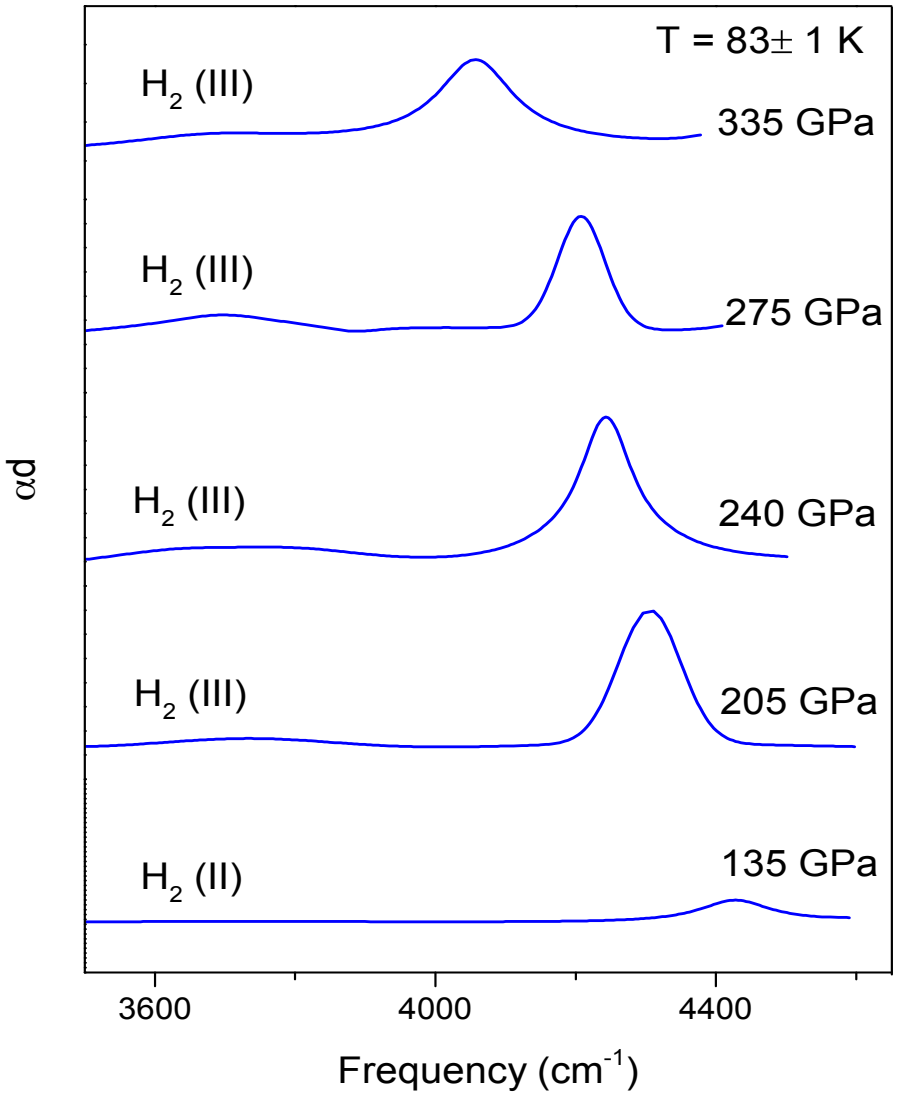

Fig. S1
IR vibron absorption peaks in solid hydrogen for several pressures. The phases are identified in parentheses.

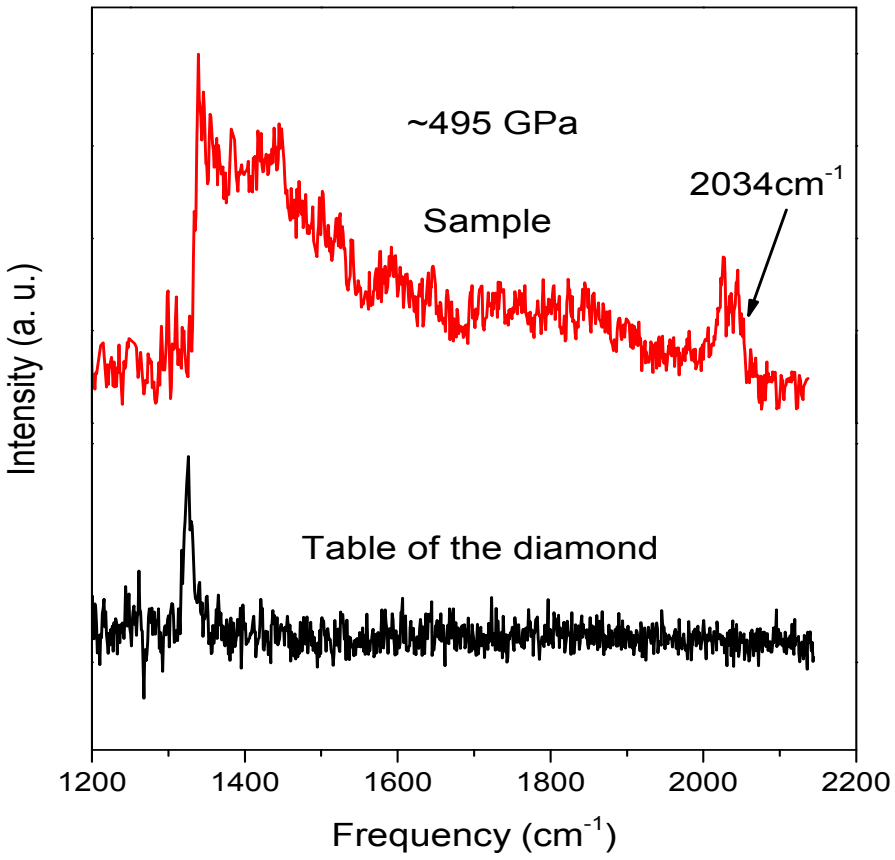

Fig. S2

The Raman shift of the diamond phonon from the culet region that presses on the metallic hydrogen sample, determined to be 495 GPa at the highest pressure. Also shown is a Raman spectrum from the unstressed table of the diamond.

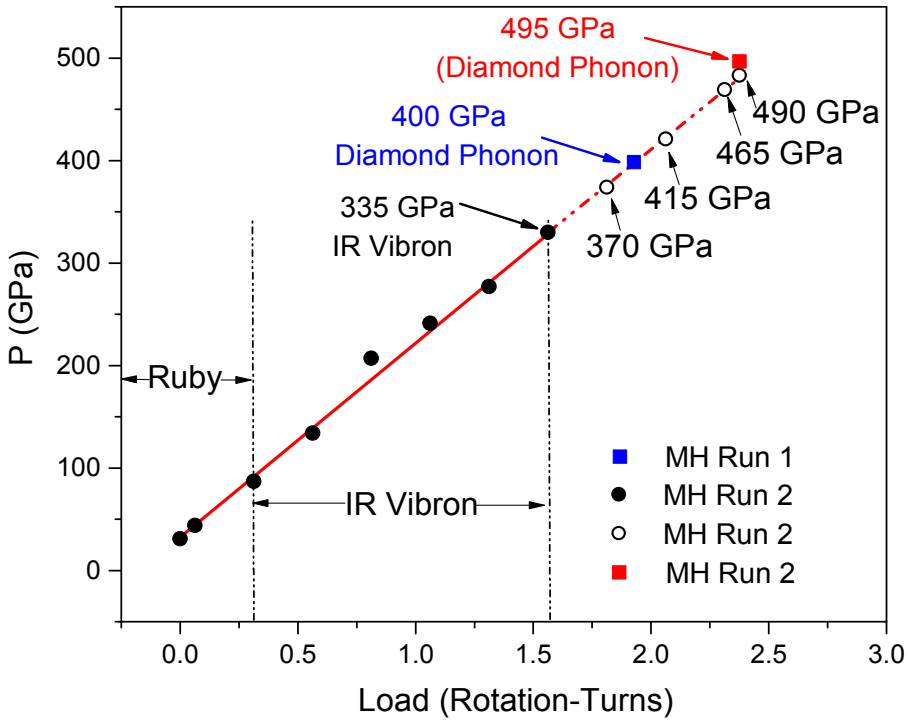

Fig. S3

Pressure as a function of load or rotation of the screw on the DAC. The solid round data points are measured pressures, confirming the linearity of the rotation scale. The solid red line shows how these points can be fit to a straight line, while the dash-dot part is an extrapolation of the load scale. The hydrogen sample was visually examined at points shown on the extrapolated line (open circles). Our experience with this secondary scale is that the rotation scale continues linearly until the increase in pressure with rotation saturates (i.e., the pressure does not increase). It is interesting that our curve has not yet saturated, which implies that the pressure can still be increased, unless the diamonds fail. The solid red square at 495 GPa is the pressure determined from the diamond Raman phonon, using the linear fit of Akahama and Kawamura. If we extrapolate their quadratic scale of 2010, the pressure is 590 GPa. In Ref. (*24*) a maximum pressure of 420 GPa was achieved, using the 2010 scale. If we revert to the Akahama-Kawamura 2006 scale that pressure would be 400 GPa, shown by the blue square. This data and our experience with our DAC using the pressure vs. load scale motivated us to use the linear scale of Akahama and Kawamura. Because our rotation scale and the 2006 scale show good agreement we have conservatively chosen to use the 2006 scale in this paper.

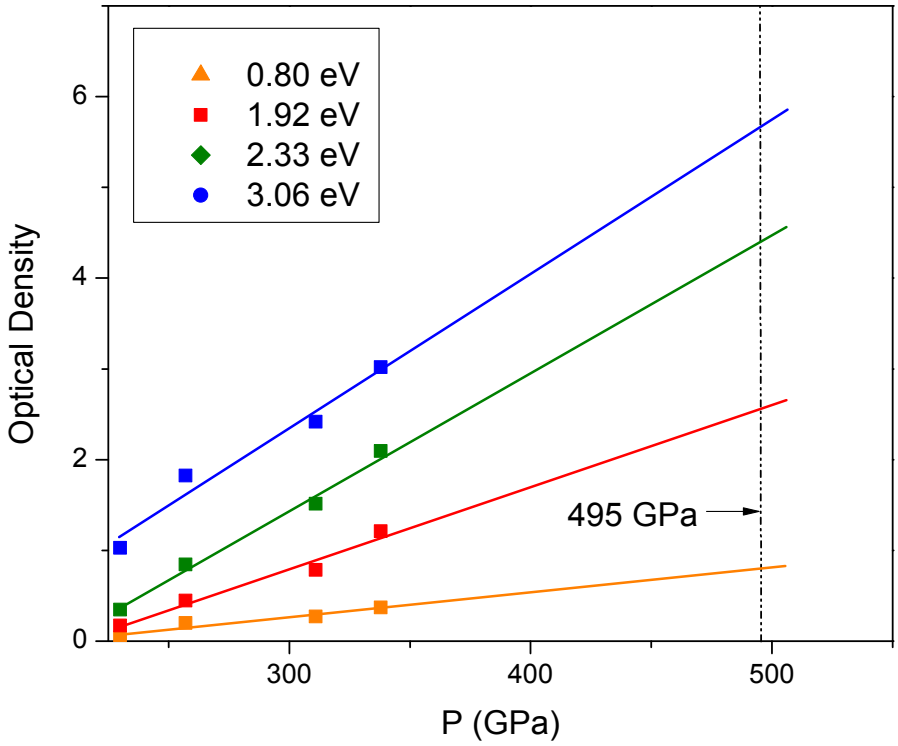

Fig. S4
The two-pass optical density of stressed diamond at high pressure used to correct the reflectance spectra for the four measured wavelengths. We have used a linear extrapolation of the data from Vohra.

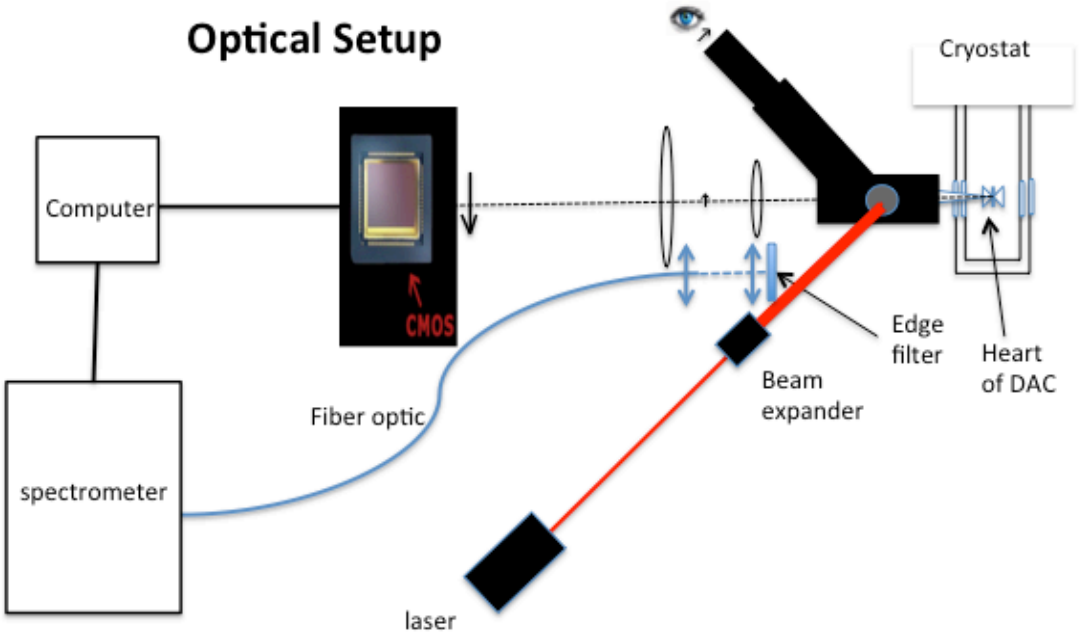

Fig. S5

The optical set-up used to photograph and measure the reflectance of the sample in the DAC. There are two CaF_2 windows between the microscope and the DAC in the cryostat.

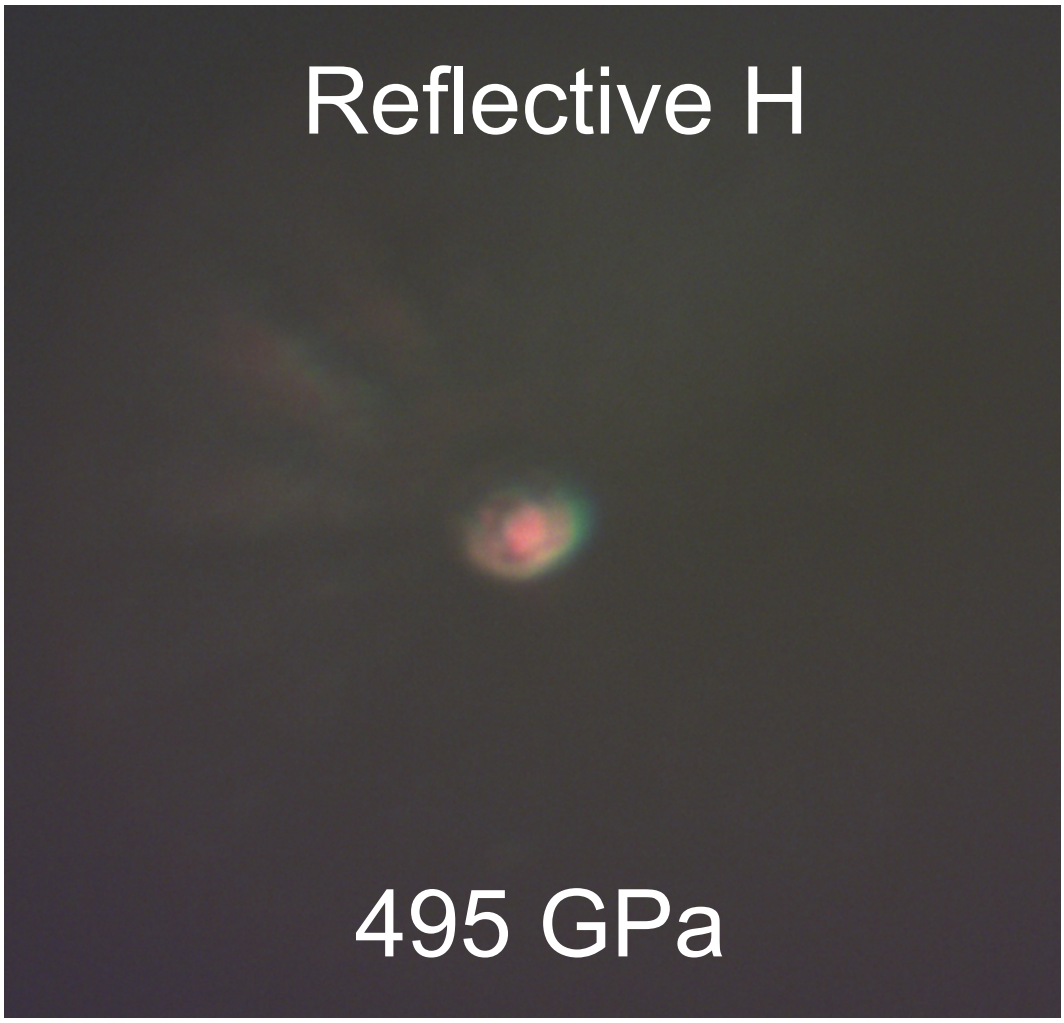

Fig. S6

Image of metallic hydrogen using the Macroscope and CMOS camera with white light illumination. The MH is approximately 10 microns in diameter. The MH has a reddish tint due to the stronger attenuation of blue light by the stressed diamond (Fig. S4). The reflectance of the MH was measured over a ˜5 micron circle. The rhenium reflectance was sampled at several points around the annulus and averaged. At very high pressures the diamond bevel region is compressed down, closer to the gasket and the focal plane. The faint radial streaks of light are due to scattered light from the diamond bevels.

A B

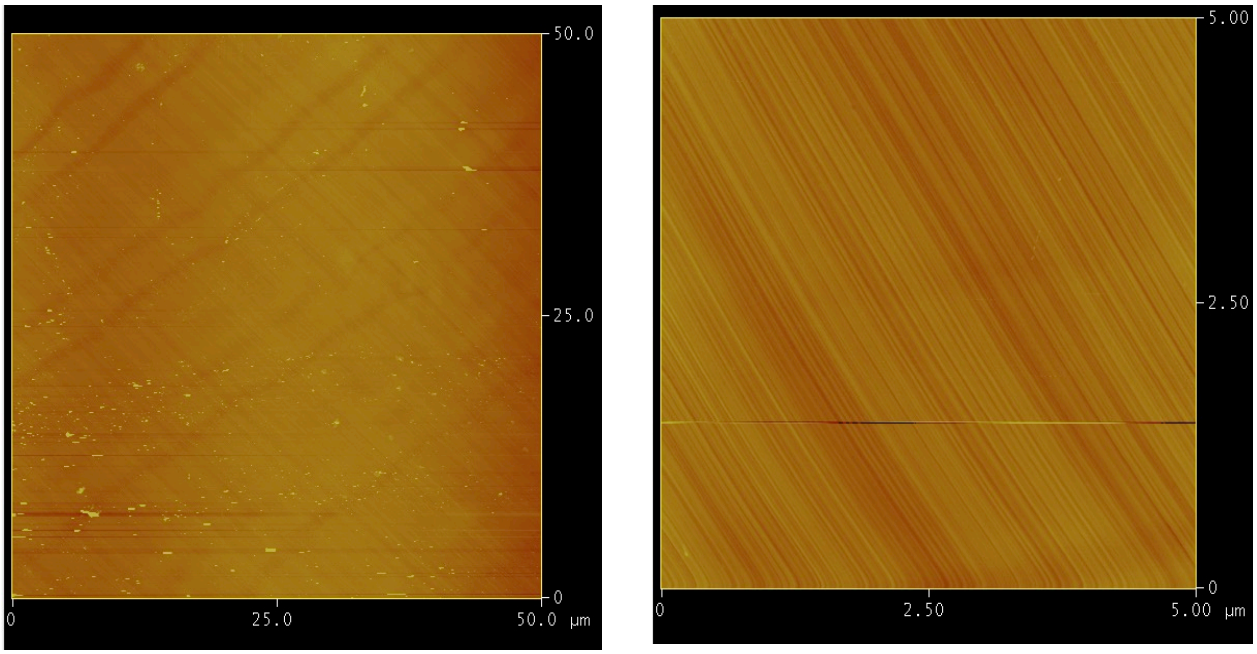

Fig. S7

AFM scans of the roughness of diamond culets. (A) A 50x50 micron^2 area showing scattered defects with a roughness of greater than 1 nm. (B) A different culet carefully polished along the grain of the diamond (diamonds have large anisotropic polishing rates) scanned over a defect free 5x5 micron^2 area with higher resolution. The roughness is less than 1 nm. Polishing striations are generally observed and are not believed to be problematic.

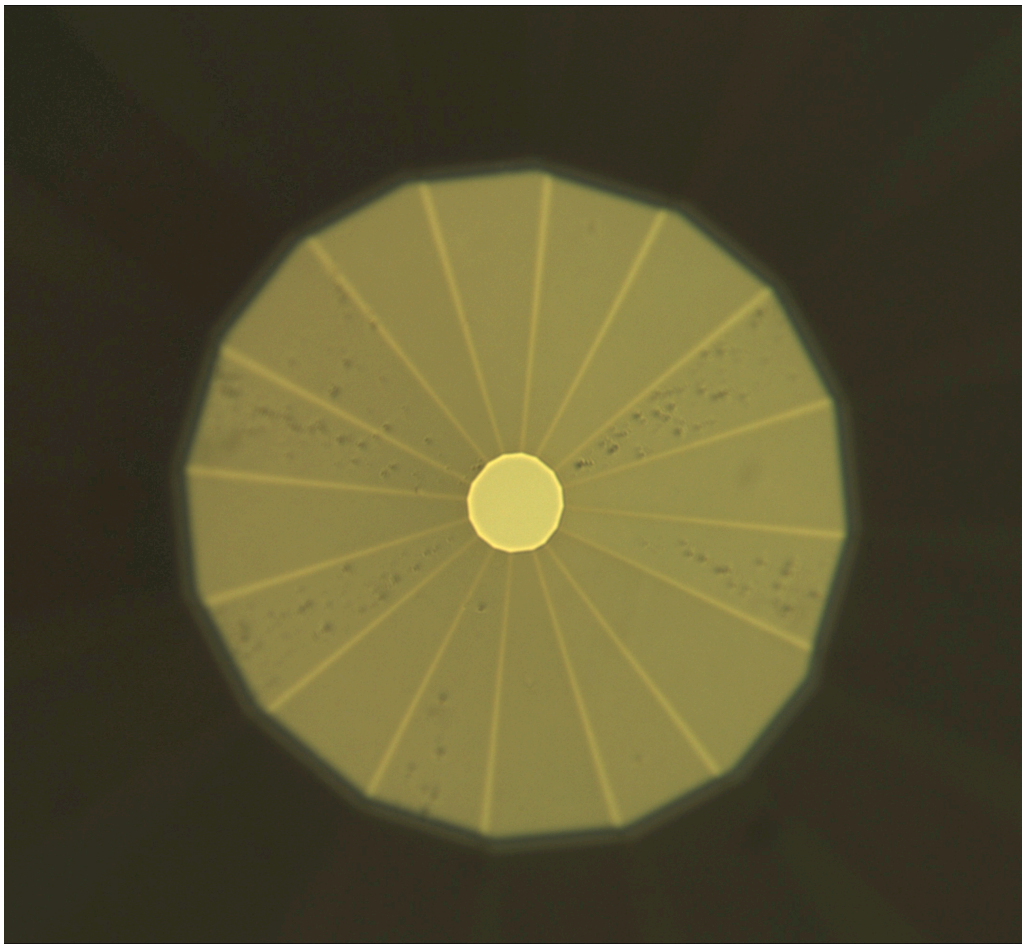

Fig. S8

A diamond with a 35 micron culet that has been etched by RIE, observed in bright field illumination. In this case the etching procedure was designed to uniformly remove atoms from the [100] culet surface. Our diamonds are beveled to a diameter of 300 microns at an angle of 8 degrees from the culet. Pitting is clearly observed on the bevels with different crystalline orientation. The stress in this region when under load in a DAC is lower than at the culet and such pitting is believed to be acceptable except near the culet edge.

Additiional Data

Fourteen data files are provided. These give information on IR spectra, load vs pressure, reflection, optical density, and Raman scattering of diamond. All files are in csv format.

References and Notes

1. V. L. Ginzburg, Nobel Lecture: On superconductivity and superfluidity (what I have and have not managed to do) as well as on the "physical minimum" at the beginning of the XXI century. *Rev. Mod. Phys.* **76**, 981–998 (2004). doi:10.1103/RevModPhys.76.981

2. E. Wigner, H. B. Huntington, On the possibility of a metallic modification of hydrogen. *J. Chem. Phys.* **3**, 764–770 (1935). doi:10.1063/1.1749590

3. J. M. McMahon, M. A. Morales, C. Pierleoni, D. M. Ceperley, The properties of hydrogen and helium under extreme conditions. *Rev. Mod. Phys.* **84**, 1607–1653 (2012). doi:10.1103/RevModPhys.84.1607

4. J. McMinis, R. C. Clay, D. Lee, M. A. Morales, Molecular to atomic phase transition in hydrogen under high pressure. *Phys. Rev. Lett.* **114**, 105305 (2015). doi:10.1103/PhysRevLett.114.105305 Medline

5. S. Azadi, B. Monserrat, W. M. C. Foulkes, R. J. Needs, Dissociation of high-pressure solid molecular hydrogen: A quantum Monte Carlo and anharmonic vibrational study. *Phys. Rev. Lett.* **112**, 165501 (2014). doi:10.1103/PhysRevLett.112.165501 Medline

6. J. M. McMahon, D. M. Ceperley, Ground-state structures of atomic metallic hydrogen. *Phys. Rev. Lett.* **106**, 165302–165304 (2011). doi:10.1103/PhysRevLett.106.165302 Medline

7. N. W. Ashcroft, Metallic Hydrogen: A High Temperature Superconductor? *Phys. Rev. Lett.* **21**, 1748–1749 (1968). doi:10.1103/PhysRevLett.21.1748

8. J. M. McMahon, D. M. Ceperley, High-temperature superconductivity in atomic metallic hydrogen. *Phys. Rev. B* **84**, 144515 (2011). doi:10.1103/PhysRevB.84.144515

9. M. Borinaga, I. Errea, M. Calandra, F. Mauri, A. Bergara, Anharmonic effects in atomic hydrogen: Superconductivity and lattice dynamical stability. *Phys. Rev. B* **93**, 174308 (2016). doi:10.1103/PhysRevB.93.174308

10. E. G. Brovman, Y. Kagan, A. Kholas, Structure of Metallic Hydrogen at Zero Pressure. *Sov. Phys. JETP* **34**, 1300–1315 (1972).

11. J. Cole, I. F. Silvera, J. P. Foote, in *STAIF-2008,* A. C. P. 978, Ed. (Albequerque, NM, 2008), vol. AIP Conf. Proc 978, pp. 977-984.

12. M. Zaghoo, A. Salamat, I. F. Silvera, Evidence of a first-order phase transition to metallic hydrogen. *Phys. Rev. B* **93**, 155128 (2016). doi:10.1103/PhysRevB.93.155128

13. S. T. Weir, A. C. Mitchell, W. J. Nellis, Metallization of fluid molecular hydrogen at 140 GPa (1.4 Mbar). *Phys. Rev. Lett.* **76**, 1860–1863 (1996). doi:10.1103/PhysRevLett.76.1860 Medline

14. V. E. Fortov, R. I. Ilkaev, V. A. Arinin, V. V. Burtzev, V. A. Golubev, I. L. Iosilevskiy, V. V. Khrustalev, A. L. Mikhailov, M. A. Mochalov, V. Y. Ternovoi, M. V. Zhernokletov, Phase transition in a strongly nonideal deuterium plasma generated by quasi-isentropical compression at megabar pressures. *Phys. Rev. Lett.* **99**, 185001–185004 (2007). doi:10.1103/PhysRevLett.99.185001 Medline

15. M. D. Knudson, M. P. Desjarlais, A. Becker, R. W. Lemke, K. R. Cochrane, M. E. Savage, D. E. Bliss, T. R. Mattsson, R. Redmer, HIGH-PRESSURE PHYSICS. Direct

observation of an abrupt insulator-to-metal transition in dense liquid deuterium. *Science* **348**, 1455–1460 (2015). doi:10.1126/science.aaa7471 Medline

16. C. Pierleoni, M. A. Morales, G. Rillo, M. Holzmann, D. M. Ceperley, Liquid-liquid phase transition in hydrogen by coupled electron-ion Monte Carlo simulations. *Proc. Natl. Acad. Sci. U.S.A.* **113**, 4953–4957 (2016). doi:10.1073/pnas.1603853113 Medline
17. G. E. Norman, I. M. Saitov, V. V. Stegailov, Plasma-Plasma and Liquid-liquid first-order phase transitions. *Plasma Phys.* **55**, 215–221 (2015). doi:10.1002/ctpp.201400088
18. I. F. Silvera, The Solid Molecular Hydrogens in the Condensed Phase: Fundamentals and Static Properties. *Rev. Mod. Phys.* **52**, 393–452 (1980). doi:10.1103/RevModPhys.52.393
19. I. F. Silvera, R. J. Wijngaarden, New Low Temperature Phase of Molecular Deuterium at Ultra High Pressure. *Phys. Rev. Lett.* **47**, 39–42 (1981). doi:10.1103/PhysRevLett.47.39
20. R. J. Hemley, H. K. Mao, Phase transition in solid molecular hydrogen at ultrahigh pressures. *Phys. Rev. Lett.* **61**, 857–860 (1988). doi:10.1103/PhysRevLett.61.857 Medline
21. H. E. Lorenzana, I. F. Silvera, K. A. Goettel, Evidence for a structural phase transition in solid hydrogen at megabar pressures. *Phys. Rev. Lett.* **63**, 2080–2083 (1989). doi:10.1103/PhysRevLett.63.2080 Medline
22. M. I. Eremets, I. A. Troyan, Conductive dense hydrogen. *Nat. Mater.* **10**, 927–931 (2011). doi:10.1038/nmat3175 Medline
23. R. T. Howie, C. L. Guillaume, T. Scheler, A. F. Goncharov, E. Gregoryanz, Mixed molecular and atomic phase of dense hydrogen. *Phys. Rev. Lett.* **108**, 125501 (2012). doi:10.1103/PhysRevLett.108.125501 Medline
24. R. Dias, O. Noked, I. F. Silvera, New Quantum Phase Transition in Dense Hydrogen: The Phase Diagram to 420 GPa. *arXiv:1603.02162v1*, (2016).
25. M. I. Eremets, I. A. Troyan, A. P. Drozdov, Low temperature phase diagram of hydrogen at pressures up to 380 GPa. A possible metallic phase at 360 GPa and 200 K. *arXiv:1601.04479*, (2016).
26. Materials and Methods are available as supplementary materials.
27. M. I. Eremets, Megabar high pressure cells for Raman measurements. *J. Raman Spectrosc.* **34**, 515–518 (2003). doi:10.1002/jrs.1044
28. P. Loubeyre, F. Occelli, R. LeToullec, Optical studies of solid hydrogen to 320 GPa and evidence for black hydrogen. *Nature* **416**, 613–617 (2002). doi:10.1038/416613a Medline
29. E. D. Palik, Ed., *Handbook of Optical Constants of Solids*, (1997), vol. III.
30. A. L. Ruoff, H. Luo, Y. K. Vohra, The closing diamond anvil optical window in multimegabar research. *J. Appl. Phys.* **69**, 6413–6416 (1991). doi:10.1063/1.348845
31. Y. K. Vohra, in *Proceedings of the XIII AIRAPT International Conference on High Pressure Science and Technology*. (1991, Bangalore, India, 1991).
32. Y. Akahama, H. Kawamura, Pressure calibration of diamond anvil Raman gauge to 310 GPa. *J. Appl. Phys.* **100**, 043516 (2006). doi:10.1063/1.2335683
33. F. Wooten, *Optical Properties of Solids*. (Academic Press, New York, 1972), pp. 260.

34. M. P. Surh, S. G. Louie, M. L. Cohen, Band gaps of diamond under anisotropic stress. *Phys. Rev. B Condens. Matter* **45**, 8239–8247 (1992). doi:10.1103/PhysRevB.45.8239 Medline

35. J. Chen, X.-Z. Li, Q. Zhang, M. I. J. Probert, C. J. Pickard, R. J. Needs, A. Michaelides, E. Wang, Quantum simulation of low-temperature metallic liquid hydrogen. *Nat. Commun.* **4**, 2064 (2013). doi:10.1038/ncomms3064 Medline

36. S. A. Bonev, E. Schwegler, T. Ogitsu, G. Galli, A quantum fluid of metallic hydrogen suggested by first-principles calculations. *Nature* **431**, 669–672 (2004). doi:10.1038/nature02968 Medline

37. S. Deemyad, I. F. Silvera, Melting line of hydrogen at high pressures. *Phys. Rev. Lett.* **100**, 155701 (2008). doi:10.1103/PhysRevLett.100.155701 Medline

38. C. Attaccalite, S. Sorella, Stable liquid hydrogen at high pressure by a novel *Ab initio* molecular-dynamics calculation. *Phys. Rev. Lett.* **100**, 114501 (2008). doi:10.1103/PhysRevLett.100.114501 Medline

39. C. S. Zha, "Hot-dense hydrogen study up to 300 GPa," presented at APS March Meeting 2016, Baltimore, MD, 17 March 2016; http://meetings.aps.org/link/BAPS.2016.MAR.V21.3.

40. E. Babaev, A. Sudbø, N. W. Ashcroft, A superconductor to superfluid phase transition in liquid metallic hydrogen. *Nature* **431**, 666–668 (2004). doi:10.1038/nature02910 Medline

41. P. Dalladay-Simpson, R. T. Howie, E. Gregoryanz, Evidence for a new phase of dense hydrogen above 325 gigapascals. *Nature* **529**, 63–67 (2016).

42. C. Kittel, *Introduction to Solid State Physics* (John Wiley & Sons, ed. 7, 1996).

43. A. Chijioke, W. J. Nellis, A. Soldatov, I. F. Silvera, The Ruby Pressure Standard to 150 GPa. *J. Appl. Phys.* **98**, 114905 (2005). doi:10.1063/1.2135877

44. H. K. Mao, J. Xu, P. M. Bell, Calibration of the Ruby Pressure Gauge to 800 kbar Under Quasi-Hydrostatic Conditions. *J. Geophys. Res.* **91** (B5), 4673–4676 (1986). doi:10.1029/JB091iB05p04673

45. C. Narayana, H. Luo, J. Orloff, A. L. Ruoff, Solid hydrogen at 342 GPa: No evidence for an alkali metal. *Nature* **393**, 46–49 (1998). doi:10.1038/29949

46. I. F. Silvera, in *AIRAPT*. (Forschungszentrum Karlsruhe http://bibliothek.fzk.de/zb/verlagspublikationen/AIRAPT_EHPRG2005/, Karlsruhe, Germany, 2005), vol. plenaries.

47. C.-S. Zha, Z. Liu, R. J. Hemley, Synchrotron infrared measurements of dense hydrogen to 360 GPa. *Phys. Rev. Lett.* **108**, 146402–146407 (2012). doi:10.1103/PhysRevLett.108.146402 Medline

48. M. Hanfland, K. Syassen, A Raman Study of Diamond Anvils under Stress. *J. Appl. Phys.* **57**, 2752–2756 (1985). doi:10.1063/1.335417

49. H. Boppart, J. van Straaten, I. F. Silvera, Raman spectra of diamond at high pressures. *Phys. Rev. B Condens. Matter* **32**, 1423–1425 (1985). doi:10.1103/PhysRevB.32.1423 Medline

50. Y. Akahama, H. Kawamura, Diamond anvil Raman gauge in multimegabar pressure range. *High Press. Res.* **27**, 473–482 (2007). doi:10.1080/08957950701659544

51. Y. Akahama, H. Kawamura, Pressure calibration of diamond anvil Raman gauge to 410 GPa. *J. Phys. Conf. Ser.* **215**, 012195 (2010). doi:10.1088/1742-6596/215/1/012195

52. B. J. Baer, M. E. Chang, W. J. Evans, Raman shift of stressed diamond anvils: Pressure calibration and culet geometry dependence. *J. Appl. Phys.* **104**, 034504 (2008). doi:10.1063/1.2963360

53. R. T. Howie, E. Gregoryanz, A. F. Goncharov, Hydrogen (deuterium) vibron frequency as a pressure comparison gauge at multi-Mbar pressures. *J. Appl. Phys.* **114**, 073505–073506 (2013). doi:10.1063/1.4818606

54. Y. K. Vohra, in *AIRAPT: Recent Trends in High Pressure Research,* A. K. Singh, Ed. (Oxford Press, New Delhi, India, 1992, Bangalore, India, 1991), vol. Proceedings of the XIII AIRAPT International Conference, pp. 349-358.

55. P. Loubeyre, R. LeToullec, D. Hausermann, M. Hanfland, R. J. Hemley, H. K. Mao, L. W. Finger, X-ray Diffraction and Equation of State of Hydrogen at Megabar Pressures. *Nature* **383**, 702–704 (1996). doi:10.1038/383702a0

56. N. W. Ashcroft, Hydrogen at high density. *J. Phys. A* **36**, 6137–6147 (2003). doi:10.1088/0305-4470/36/22/341

57. G. W. Collins, P. Celliers, D. M. Gold, M. E. Foord, R. J. Wallace, A. Ng, S. V. Weber, K. S. Budil, R. Cauble; Da Silva LB, Measurements of the equation of state of deuterium at the fluid insulator-metal transition. *Science* **281**, 1178–1181 (1998). doi:10.1126/science.281.5380.1178 Medline

58. P. M. Celliers, G. W. Collins, L. B. Da Silva, D. M. Gold, R. Cauble, R. J. Wallace, M. E. Foord, B. A. Hammel, Shock-induced transformation of liquid deuterium into a metallic fluid. *Phys. Rev. Lett.* **84**, 5564–5567 (2000). doi:10.1103/PhysRevLett.84.5564 Medline

59. G. W. Collins, P. M. Celliers, L. B. Da Silva, R. Cauble, D. M. Gold, M. E. Foord, N. C. Holmes, B. A. Hammel, R. J. Wallace, A. Ng, Temperature measurements of shock compressed liquid deuterium up to 230 GPa. *Phys. Rev. Lett.* **87**, 165504 (2001). doi:10.1103/PhysRevLett.87.165504 Medline

60. P. Loubeyre, S. Brygoo, J. Eggert, P. M. Celliers, D. K. Spaulding, J. R. Rygg, T. R. Boehly, G. W. Collins, R. Jeanloz, Extended data set for the equation of state of warm dense hydrogen isotopes. *Phys. Rev. B* **86**, 144115 (2012). doi:10.1103/PhysRevB.86.144115